Applied Thermal Engineering 258 (2025) 124557

Contents lists available at ScienceDirect

Applied Thermal Engineering

journal homepage: www.elsevier.com/locate/apthermeng

Research Paper

Calcium chloride dihydrate as a promising system for seasonal heat storage in a suspension reactor

Lena Schmieder *, Selma Kuloglija, Katsiaryna Ilyina-Brunner, Sandra Jezernik, Franz Winter

Institute of Chemical, Environmental and Bioscience Engineering, Technische Universität Wien, Vienna, Austria

ARTICLE INFO

Keywords:
Thermochemical energy storage
Three-phase suspension reactor
Calcium chloride
Salt hydrates
Cycle stability
Thermal oil

ABSTRACT

The shift to renewable energy sources increases the demand for energy storage to balance supply and demand. The call for heat storage solutions is particularly high with heat dominating residential energy needs. Simultaneously, significant industrial waste heat potential could be seasonally stored in reversible chemical reactions using thermochemical energy storage technologies. This study investigates the reversible dehydration of calcium chloride dihydrate which has been recognised as a suitable thermochemical material in prior studies. A new method is introduced by investigating the reaction in a lab-scale batch-type suspension reactor. In the reactor, a mechanical stirrer suspends the solid thermochemical material in an inert liquid, to prevent agglomeration of the particles. The investigation involves a parameter variation that includes different suspension media, different mass fractions of the solid reactant, as well as different system pressures during charging. The experimental investigation renders 40 wt% solid or lower as the most promising mass fraction to avoid agglomeration. Vegetable oils show promising results as suspension media. However, they lack thermal stability in the temperature range of up to 210 °C. Mineral oil can ensure thermal and cycle stability. Furthermore, a notable reduction in the dehydration reaction temperatures (176 to 109 °C) is observed when the system pressure is decreased down to 50 mbar. The study concludes that calcium chloride dihydrate has the potential to be used for 22 stable charging and discharging cycles in a mineral oil suspension and that lowering the system pressure can reduce the required charging temperature of the system. To further enhance the suspension method, it is essential to focus on mass transfer and foam mitigation during the dehydration reaction.

1. Introduction

1.1. Need for heat storage and waste heat potentials

The phenomenon of global warming puts considerable pressure on the energy-providing sector to transition to renewable energy sources and to reduce CO_2 emissions. Therefore, the renewable energy sector is experiencing rapid growth, with renewable electricity expected to account for a third of global power generation by 2025. Renewable heat production on the other hand is only expected to make up 12 % of global heat use by then. Without a significant reduction in the use of non-renewable heat, CO_2 emissions from heating are forecasted to drop by just 2 % from 2019 levels [1]. Simultaneously, in the EU-27 industries, approximately one-third (29 %) of energy consumption is lost in waste heat, representing a significant potential for heat storage. The lost energy amounts to 3,300 PJ in the EU-27, with 51 % being low-temperature heat, below 100 °C [2]. The global waste heat potential is even more significant, with 52 % (245,000 PJ) of energy being lost as exhaust heat, of which 63 % is in the low-temperature range [3]. This justifies further research into storage systems that function at this temperature level. The project, this research is part of, is focused on storing heat in the low- to mid-temperature range up to 210 °C.

1.2. Thermal energy storage principles

There are different thermal energy storage (TES) methods, which can be divided into three categories according to the underlying working principle.

Sensible heat storage. The currently most used heat storage method with the highest technology readiness level (TRL) of 9–11 is sensible heat storage [4]. Heat is stored in a solid or liquid material by simply heating it up and then storing it in an insulated compartment. Examples of sensible heat storage include water, soil or gravel and the technology

* Corresponding author.
E-mail addresses: lena.schmieder@tuwien.ac.at (L. Schmieder), selma.kuloglija@tuwien.ac.at (S. Kuloglija), sandra.jezernik@tuwien.ac.at (S. Jezernik), franz.winter@tuwien.ac.at (F. Winter).

https://doi.org/10.1016/j.applthermaleng.2024.124557
Received 22 December 2023; Received in revised form 1 September 2024; Accepted 3 October 2024
Available online 5 October 2024

Nomenclature

Symbols

T (K)	temperature
T (°C = K − 273.15)	temperature
Δh_R (J/mol)	reaction enthalpy
T (s)	time
K (−)	equilibrium constant
ΔT (K or °C)	temperature difference
P (bar = 10^5 Pa)	pressure
p^+ (bar = 10^5 Pa)	reference pressure
$p_{B/H2O}$ (bar = 10^5 Pa)	partial pressure of component B/H_2O
$\Delta_R H°$ (J/mol)	enthalpy at standard conditions
$\Delta_R S°$ (J/(molK))	entropy at standard conditions
R (J/(molK))	ideal gas constant
N (−)	stochiometric factor
$v(H_2O)$ (ml)	volume of water
X_i (−)	conversion

Abbreviations

wt%	weight percentage
(g)	gaseous
(l)	liquid
(s)	solid
TES	thermal energy storage
TRL	technology readiness level
PCM	phase change material
TCES	thermochemical energy storage
SHS	sorption heat storage
CRHS	chemical reaction heat storage
TCM	thermochemical material
TGA	thermogravimetric analysis
STA	simultaneous thermal analysis
CAS	Chemical Abstracts Service
OFAT	one factor at a time
PLC	programmable logic controller
RTD	residence time distribution
CSTR	continuously stirred tank reactor
Max	maximum
Start	start of charging reaction
TCES	thermochemical energy storage
TCM	thermochemical material
TRL	technology readiness level
OFAT	one factor at a time

is mostly suitable for short-term storage because it deals with heat loss and self-discharge over time [5]. Additionally, this technology has the lowest energy storage densities at around 0.18 GJ/m^3 [6].

Latent heat storage. The second method, latent heat storage, increases the storage capacity of sensible heat storage to approximately 0.38 GJ/m^3 by inducing a phase change in addition to raising the temperature of the material [6]. As a result, latent heat storage not only retains the sensible heat but also stores energy in the form of latent heat of fusion or latent heat of vaporisation, depending on the phase change involved. The materials used can be either organic or inorganic and typically the phase change from solid to liquid state of so-called phase change materials (PCM) is used. This form of heat storage has already been investigated quite well, sitting at TRL 8–9 but still requires insulation as it suffers from heat losses and is mostly used for short to medium-term storage [4,5].

Thermochemical energy storage. This work focuses on the third option of storing heat in the form of enthalpy in either a sorption process or chemical reaction. This form of TES is called thermochemical storage (TCES) and can be divided into the subgroups of sorption heat storage (SHS) and chemical reaction heat storage (CRHS) [7]. CRHS uses reversible endo- and exothermic reactions, like the one described in Eq. (1):

$$A_{(s)} \longleftrightarrow^{\pm \Delta H_R} B_{(s)} + C_{(g/l)} \quad (1)$$

During the endothermic charging process, the solid educt A is heated until the reaction temperature is reached. It then dissociates to form solid product B and gaseous product C. The resulting components are stored separately until the heat is required again, with minimal thermal losses apart from those associated with sensible heat transfer. During the exothermic discharging reaction, the educts B and C are once again combined to form the solid product A, releasing the previously stored enthalpy as heat, which can be utilised. Provided that B and C are stored separately, there is no possibility of self-discharge, which renders TCES the optimal method for TES over extended periods, up to seasons and even years [5]. A possible reaction for this application is the reversible dehydration of salt hydrates [8].

1.3. Seasonal heat storage options

Since heat demand not only varies hourly or daily but also seasonally storing excess heat from summer up until the winter months is of particular interest. The mentioned TES methods all offer seasonal storage solutions. Underground sensible heat storage in boreholes and aquifers is an option to store heat seasonally at around 80 °C. Boreholes store heat in rocks or soil with low thermal conductivity, which minimises losses [9]. Aquifers store natural groundwater and are constrained by low initial water temperatures. However, following the initial discharge, they can be recharged in summer for domestic use [10,11]. In latent heat storage, sub-cooled PCMs such as erythritol-containing sugar alcohols can be an option for long-term heat storage at 70 °C to 100 °C. [12] Thermochemical energy storage using salt hydrates is generally suitable for seasonal storage, as the charged reaction partners can be kept separate until the heat is needed again during discharging [13]. As mentioned, no insulation is needed as the heat is stored in chemical bonds.

1.4. Calcium chloride dihydrate

Thermochemical material. Several requirements need to be considered when selecting a suitable thermochemical material (TCM). Examples include low cost, high-energy density, cycle stability (the ability of the material to withstand many dehydration-hydration cycles), safety, suitable reaction temperature, high conversion and low corrosivity. Calcium chloride ($CaCl_2$) has high potential as a TCM due to its low cost, high availability and low safety risks [14].

It can form various hydrates $CaCl_2 \cdot n\ H_2O$ with n = {0,1,2,4,6} [15]. This work uses the reversible reaction of the dihydrate $CaCl_2 \cdot 2\ H_2O$ to the anhydrate $CaCl_2$ as the hexahydrate and tetrahydrate have melting points of 30 °C and 45 °C [15], respectively and therefore do not suit the application. Thermogravimetric analysis (TGA) measurements at 450 mbar suggest that during charging (dehydration), the first reaction step, shown in Eq. (2), occurs at 160 °C. The second step to the anhydrate, according to Eq. (3) takes place at 200 °C [16].

$$CaCl_2 \cdot 2H_2O_{(s)} \rightarrow CaCl_2 \cdot H_2O_{(s)} + H_2O_{(g/l)} \quad (2)$$

$$CaCl_2{\cdot}H_2O_{(s)} \rightarrow CaCl_{2(s)} + H_2O_{(g/l)} \quad (3)$$

The discharging (hydration) mechanism is believed to be a three-step reaction and proceeds as shown in Eqs. (4)–(6) [16]

$$CaCl_{2(s)} + 0.3\ H_2O_{(g/l)} \rightarrow CaCl_2{\cdot}0.3H_2O_{(s)} \quad (4)$$

$$CaCl_2{\cdot}0.3H_2O_{(s)} + 0.7\ H_2O_{(g/l)} \rightarrow CaCl_2{\cdot}H_2O_{(s)} \quad (5)$$

$$CaCl_2{\cdot}H_2O_{(s)} + H_2O_{(g/l)} \rightarrow CaCl_2{\cdot}2H_2O_{(s)} \quad (6)$$

Different properties of the calcium chloride hydrates are shown in Table 1, showing e.g. that the melting points of these components fit the application. Additionally, the Chemical Abstracts Service (CAS) number is given to identify the materials.

$CaCl_2{\cdot}2\ H_2O$ in TCES. As TCES systems using salt hydrates often face the problem of agglomeration [19,20] the majority of investigations avoid the use of calcium chloride on its own but rather incorporate additional host materials like aluminosilicates or expanded graphite to enhance the structural stability [19,21,22]. Another option that combines physisorption with the chemical reaction is adding solid adsorbents like zeolites, metal–organic frameworks and silica gel [21,23,24].

While *Nonnen et al.* [24] developed an open adsorption system with a moving material bed using zeolite Ca-X and 15 wt% $CaCl_2$ and achieved energy storage density of up to 0.936 GJ/m^3, *Courbon et al.* [23] reached an energy storage density of 0.760 GJ/m^3 with a silica gel and 43 wt% $CaCl_2$ composite material that was planned to be tested in a prototype.

Another extensively researched composite material with calcium chloride is vermiculite. In their study, *Aydin et al.* [25] introduced an open-sorption pipe system using vermiculite and $CaCl_2$. The system achieved an energy storage density of 1.04 GJ/m^3. *Casey et al.* [26] developed an open system fixed bed using vermiculite and 56 wt% $CaCl_2$ with meshed tube air diffusers and reached an energy density of 0.404 GJ/m^3. *Aydin et al.* [27] also investigated a hybrid system combining a solid sorption heat storage with an air-sourced heat pump. The most promising composite material was 43 wt% $CaCl_2$ providing an energy density of 0.612 GJ/m^3. They also found that modifying $CaCl_2$ with LiCl enhances both heat output during hydration and moisture removal during charging. *Rammelberg et al.* [28] also tested salt hydrate mixtures, among them the mixture of $CaCl_2$ and $MgCl_2$ salt hydrates. They found that mixing can improve cyclability but also concluded that further research into the optimal mixing ratio is needed.

Recently, microencapsulation of salt hydrates into materials such as hydrophobic polymers and hydrophilic hollow silica to tackle agglomeration has gained interest [29,30]. Currently these methods still need high amounts of material to achieve the effect which decreases the energy densities to below 1 GJ/m^3. *Barsk et al.* [20] developed modified dry water-style preparation methods for leakage-free microencapsulation of $CaCl_2$ with hydrophobic fumed silica nanoparticles using 98 wt% $CaCl_2$. They achieved theoretical volumetric energy storage densities up to 1.4 GJ/m^3 and cycle stability over 30 cycles in simultaneous thermal analysis (STA) which is yet to be proven in a prototype.

A new approach. However, these mentioned practices add additional costs and complexity and are yet to be proven on a larger scale [21,29]. Developing further methods to prevent agglomeration while maintaining high energy density is crucial, alongside proving the feasibility of innovative reactor designs [19,21] The research conducted in this work aims to avoid agglomeration and improve heat and mass transfer by introducing an additional inert liquid phase to achieve the positive effects of the host matrix without a preparation step of the material. Additionally, an innovative overall reactor concept in the field is chosen as explained in the following chapter.

Table 1
Properties of calcium chloride anhydrate, monohydrate and dihydrate [17,18].

		$CaCl_2$	$CaCl_2{\cdot}H_2O$	$CaCl_2 \cdot 2\ H_2O$
CAS number		10043–52–4	22691–02–7	10035–04–8
Molar mass	kg/mol	110.99	129.01	147.02
Melting point	°C	772	260	176
Density (25 °C)	kg/m^3	2220	2240	1850
Specific heat (hydrate)	kJ/(kgK)	0.670	0.840	1.170

1.5. Reactor designs in thermochemical energy storage

Reactor types in TCES. Even though the number of publications in the field of chemical reaction heat storage has doubled from 2016 to 2022 [7], it is still a rather new research area at TRLs of 1–4 [31]. This results in most of the investigated solid–gas reaction systems in the temperature range of 50–250 °C only being tested on a laboratory scale so far [6]. The most used reactor concepts are different configurations of fixed/packed reactors, moving bed reactors and fluidised bed reactors [19,32]. In implementing the TCES technology, the development of a reactor design ensuring optimal heat and mass transfer and preventing agglomeration issues remains imperative [19,21,33]. Three-phase suspension reactors stand out for their advantages in these areas [34]. *Zondag et al.* [35] conducted a brief investigation utilising calcium chloride in an unspecified inert liquid, revealing challenges related to suspension stability. The reactor employed in the work at hand addresses this issue by integrating a mechanical stirrer to ensure stability. Stirred tanks are noted for their homogeneous temperature distribution [34] and offer the possibility of discharge using liquid water due to the quick, homogeneous distribution. Additionally, they are well suited for scale-up and can be cost effective due to their simple design [36,37].

Open or closed system. TCES systems using salt hydrates like calcium chloride dihydrate can be operated in two different ways: as an open or closed system [38,39]. In a closed system, the TCM and the gaseous component (water vapour) are located within the same plant, while in the open system, the gaseous component is decoupled. As water is non-toxic and already exists in the environment it can be released during charging and provided from outside the system during discharging. This could mean that the water does not have to be stored during the seasonal storage phase. Closed systems require more complicated process engineering but allow a free choice of operating pressures. A challenge of closed systems is the gas flow between the reactor and the storage tank. This is made possible by implementing a condenser/evaporator unit with an attached storage tank [39]. The lab-scale batch reactor used in this work is operable as either an open or a closed system during charging allowing the alteration of the system pressure. It is operated as an open system during discharging, as the water is brought in from outside the reactor unit.

1.6. Energy storage density in oil

When storing heat, it is essential that the chosen TCES system can ensure a high energy storage density. To determine the potential energy storage density of the $CaCl_2 \cdot 2\ H_2O - CaCl_2$ system, the reaction enthalpy of the mentioned reactions is calculated using the standard enthalpies of formation of the components, listed in Table 2. The reaction enthalpy can be calculated for liquid and gaseous water.

Table 2
Standard enthalpies of formation and calculated reaction enthalpies [18].

Standard enthalpy of formation $\Delta_f H^0$		
$CaCl_{2(s)}$	kJ/mol	−795.39
$CaCl_2 \cdot 2\ H_2O_{(s)}$	kJ/mol	−1396.62
$H_2O_{(l)}$	kJ/mol	−285.83
$H_2O_{(g)}$	kJ/mol	−241.83
Reaction enthalpy $\Delta_R H$		
$CaCl_{2(s)} + 2\ \mathbf{H_2O_{(l)}} \longleftrightarrow CaCl_2 \cdot 2\ H_2O_{(s)}$	kJ/mol	(−)29.57
$CaCl_{2(s)} + 2\ \mathbf{H_2O_{(g)}} \longleftrightarrow CaCl_2 \cdot 2\ H_2O_{(s)}$	kJ/mol	(−)117.58

Showing the energy storage densities in the commonly used unit J/$m^3_{(higher\ hydrate)}$ gives the values 1.480 GJ/$m^3_{(CaCl2\ \cdot\ 2\ H2O)}$ for gaseous and 0.372 GJ/$m^3_{(CaCl2\ \cdot\ 2\ H2O)}$ for liquid water per m^3 of calcium chloride dihydrate using the solid density of the salt hydrate. Since the salt is usually present as a powder the bulk density is determined after DIN ISO 60 using a standardised funnel. The expected and experimental densities are listed in Table 3. The energy density using the bulk density of the salt is significantly lower at 0.686 GJ/$m^3_{(CaCl2\ \cdot\ 2\ H2O)}$ for gaseous and 0.173 GJ/$m^3_{(CaCl2\ \cdot\ 2\ H2O)}$ for liquid water. Tapping the salt to further compact it leads to a tapped density of 1022 kg/m^3 and volumetric energy densities of 0.817 GJ/$m^3_{(CaCl2\ \cdot\ 2\ H2O)}$ for gaseous and 0.206 GJ/$m^3_{(CaCl2\ \cdot\ 2\ H2O)}$ for liquid water.

The energy densities of the suspension using different oils is calculated using the densities of the oils from Table 7 and the solid density of calcium chloride dihydrate as listed in Table 3. The mixing density of a suspension containing a mass fraction of w_{solid} calcium chloride dihydrate is calculated as

$$\rho_{suspension} = \frac{1}{\frac{w_{solid}}{\rho_{solid}} + \frac{1-w_{solid}}{\rho_{oil}}} \tag{7}$$

The actual suspension densities, listed in Table 4 are measured at 25 °C by filling a compartment of known volume with the suspension, carefully scraping the excess off with a ruler and then measuring the weight with a precision scale. The solid density in Table 3 is determined similarly, but using a more precise pycnometer and the known oil volume to retract the solid density from Eq. (7).

The oil content not only decreases the density of the material but also reduces the concentration of the reactive material which further decreases the volumetric energy density. Therefore, keeping the oil content low is important. For further scale-up of the system, a separation unit and oil circulation are considered to reduce the oil content before the suspension enters the storage tank [41]. Table 3 and Table 4 also show that the energy density using a suspension of 70 wt% solid (and therefore only 30 wt% oil) can ensure similar volumetric energy densities to the tapped density of the salt.

The difference in reaction enthalpy between the reactions with liquid and gaseous water is challenging for low-temperature TCES systems. Using water vapour for the hydration reaction ensures higher reaction enthalpies and energy densities but requires additional energy input to evaporate said water for discharging. This is not desirable in the context of seasonal charging-discharging cycles. Therefore, the hydration reaction using liquid water is chosen for this work, ensuring easier handling in the current setup.

2. Materials and methods

2.1. Dehydration and hydration in oil

As mentioned in the introduction this work explores the approach of using a suspension medium to improve heat transfer and avoid agglomeration of the TCM particles. To stabilise the suspension a lab-scale reactor in the style of a stirred tank is used. A mechanical stirrer is implemented to suspend the solid TCM in an inert liquid, in this case, a thermal oil.

During the dehydration of the TCM (charging of the system), the suspension is heated and the crystal water leaves the salt in the form of water vapour bubbles rising to the suspension surface. This process is shown in the schematic in Fig. 1(a). During the hydration reaction (discharging of the system), depicted in Fig. 1(b), water is added in liquid form via a syringe to ensure the formation of small droplets.

Table 4
Calculated and experimentally determined suspension densities and the corresponding volumetric energy densities using different solid weight fractions and oils.

Oil	w_{solid}	suspension density		energy density $H_2O_{(l)}$		energy density $H_2O_{(g)}$	
		calc.	exper.	calc.	exper.	calc.	exper.
		kg/m^3	kg/m^3	GJ/m^3	GJ/m^3	GJ/m^3	GJ/m^3
Mineral	0.3	1031	1062	0.062	0.064	0.247	0.255
	0.7	1373	1388	0.193	0.195	0.769	0.777
Silicone	0.3	1120	1127	0.068	0.068	0.269	0.270
	0.7	1439	1442	0.203	0.203	0.806	0.807
Rapeseed	0.3	1080	1122	0.065	0.068	0.259	0.269
	0.7	1411	1420	0.199	0.200	0.790	0.795
Sunflower	0.3	1080	1090	0.065	0.066	0.259	0.262
	0.7	1411	1360	0.199	0.192	0.790	0.761

2.2. Experimental setups and procedures

This work uses three different experimental setups to investigate different solid mass fractions w_{solid} and suspension media (Setup 1a), cycle stability (Setup 1b) and system pressure variation (Setup 2). The main varied and fixed technical parameters of the different setups and the experiments conducted in them are summarised in Table 5.

Setup 1a (Batch reactor). The first setup, the double-walled batch reactor with mantle heating is shown in Fig. 2. The reactor ($CaCl_2 \cdot 2\ H_2O$ and thermal oil) is heated by a heating bath circulation thermostat (Huber CC-308B) containing a service oil. A heating profile, explained in Chapter 2.4, is set on the thermostat to ensure reproducible experiments and the OFAT (one factor at a time) method is used to test the influence of parameters like w_{solid} and the choice of thermal oils. The heated reactor volume of 800 ml is filled with ~550 ml of suspension to allow excess space for the expansion of the oil at higher temperatures and foam formation. The solid reactant is suspended by a propeller stirrer, the speed of which is adjusted to fully suspend the particles in the oil. Therefore, the stirrer speed is increased at higher solid mass fractions. During dehydration, the suspension is heated, and the reactor is gassed with nitrogen at the lid to protect the suspension from contact with air and to quickly remove the formed water vapour from the reaction zone. The water vapour then exits through the distilled link (heated to avoid premature condensation) and reaches the cooler, where it condenses and drips down into a water collector. The volumetric scale of the burette allows an overview of the reaction progress. A thermocouple (type K) is used to measure the temperature inside the suspension.

Setup 1b (Improved batch reactor). For the extensive cycle stability

Table 3
Calculated and experimentally determined salt densities and the corresponding volumetric energy densities.

Salt density	Density		Energy density $H_2O_{(l)}$		Energy density $H_2O_{(g)}$	
	calc.	exper.	calc.	exper.	calc.	exper.
	kg/m^3	kg/m^3	GJ/m^3	GJ/m^3	GJ/m^3	GJ/m^3
Solid density	1850 [18]	1835	0.372	0.369	1.480	1.468
Bulk density	835 [40]	858	0.168	0.173	0.668	0.686
Tapped density	–	1022	–	0.206	–	0.817

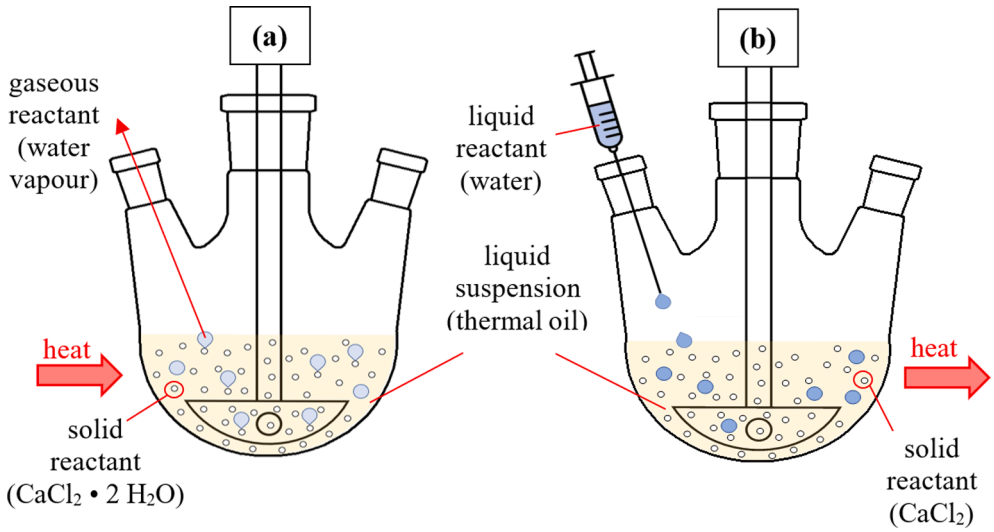

$$CaCl_2 \cdot 2\ H_2O_{(s)} + \Delta h_R \leftrightarrow CaCl_{2(s)} + 2\ H_2O_{(g/l)}$$

Fig. 1. Schematic of the three phases in a three-necked flask during dehydration (a) and hydration (b) of calcium chloride.

Table 5
Main technical parameters of the setups and experiments.

Setup	Parameter	fixed/ varied	value
Setup 1a and 1b	reactor volume (heated)	fixed	800 ml
	reactor aspect ratio H:D	fixed	10:10
	stirrer type	fixed	propeller stirrer
	nitrogen stream	fixed	0.2 ml/min
	heating profile	fixed	s. Fig. 3
	pressure	fixed	ambient
	water addition speed	fixed	18 ml/min
	water temperature	fixed	room temperature
	amount of water	fixed	stochiometric
Setup 1a	suspension volume (25 °C)	fixed	~550 ml
	suspension aspect ratio H:D	fixed	8:10
	solid mass fraction	varied	30–70 wt%
	stirrer speed	varied	300–500 rpm
	suspension medium	varied	s. Table 7
Setup 1b	suspension volume (25 °C)	fixed	~300 ml
	suspension aspect ratio H:D	fixed	6:10
	solid mass fraction	fixed	30 wt%
	stirrer speed	fixed	300 rpm
	suspension medium	fixed	mineral oil
Setup 2	flask volume	fixed	500 ml
	suspension volume (25 °C)	fixed	~200 ml
	stirrer type	fixed	stirring paddle
	solid mass fraction	fixed	30 wt%
	stirrer speed	fixed	300 rpm
	suspension medium	Fixed	mineral oil
	pressure	varied	50–1013 mbar

tests over 25 runs, Setup 1 is changed slightly to allow automatic tracking of the amount of condensed water. A load cell is attached to the programmable logic controller (PLC) and a sample tube is placed under the cooler, instead of the water collector, allowing continuous tracking of the weight of the water that condenses and drips down into the tube. The reference value for the heating profile is changed from the internal temperature of the thermostat to a temperature sensor (Pt100) inside the suspension, replacing the thermocouple (type K) to improve accuracy

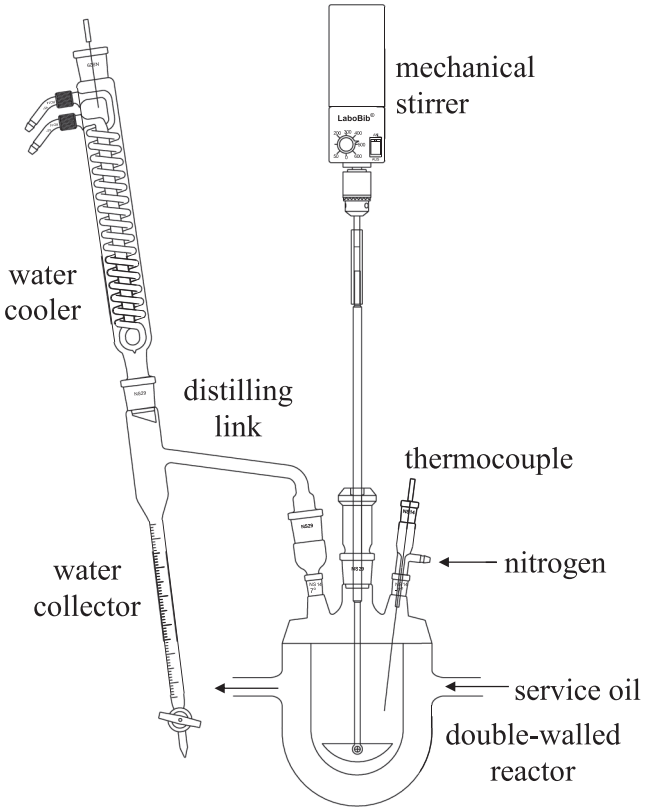

Fig. 2. Experimental setup batch reactor (Setup 1a).

and allow better control of the suspension temperature. The improved heating profile is shown in Chapter 2.4.

Setup 2 (Three-necked flask). This experimental setup replaces the reaction vessel with a three-necked flask in a service oil bath to allow better insight into the reaction zone during system pressure variation. The oil used for this type of experiment is mineral oil. The 500 ml flask is filled with 200 ml of suspension, which is heated by a service oil bath placed on a heating plate. The heating is regulated manually and temperature is measured inside the suspension using a thermocouple (type

K). To lower the system pressure a vacuum pump (Welch Ilmvac Membrane pump VAKUUM SYSTEM LVS 310 Zp economic) is attached at the cooler outlet. In addition to the pressure sensor inside the pump, a pressure gauge is installed to measure the pressure inside the reaction zone.

Hydration reaction. Once the reactor is cooled down to room temperature (~24 °C) the hydration reaction is performed by adding liquid water using a syringe. The reactor is not insulated to visibly judge the change in consistency and possibly occurring agglomeration. The temperature is recorded, and the maximum temperature rise is documented to see possible changes over multiple dehydration-hydration cycles. The amount of water added corresponds to the stoichiometric amount of water bound in the hydrated solid material. For 75 g of $CaCl_2 \cdot 2\,H_2O$ before dehydration this value would be 18.4 ml of water, which is added at a rate of ~18 ml/min. Water temperature (~23 °C) and addition rate are kept the same each cycle.

2.3. Measured data

Temperature. Setup 1a and 1b continuously keep track of the temperature inside the flask or reactor. This enables the temperature rise during discharging to be recorded and allows the starting and maximum temperatures of the charging reaction to be determined. When determining the charging reaction's starting temperatures in Setup 2, the value is taken at which the first bubbles are formed in the suspension. The uncertainties of the temperature element and the acquisition device need to be added up and result in ±4.5 °C for Setup 1a and ±0.3 °C (for the temperature rise) for Setup 1b. The errors are listed in Table 6.

Pressure. When lower pressure is applied to the reactor using a membrane vacuum pump, the system pressure is measured and displayed at two points in the system, directly at the adjustable vacuum pump and inside the reactor. The vacuum pump of the company Welch Ilmvac is self-regulated and can be set to a desired point, which it will hold using a two-point control. It will switch on to readjust the pressure once the system pressure exceeds the setpoint by 10 mbar. The accuracy of the sensor is given in Table 6. The additional measurement device, in the reaction zone, is used to ensure that the system pressure measured by the pump is present in the reactor. The noted pressure is the one displayed by the pump and has an accuracy of ±2 mbar.

Conversion. The condensed water during dehydration is measured volumetrically $V_{condensed}$ (Setup 1a) or gravimetrically $m_{condensed}$ (Setup 1b). Dividing the resulting value by the stoichiometric amount of water in the solid phase $V_{stoichiometric}$ or $m_{stoichiometric}$ shows the conversion X_i of the reaction:

$$X_i = \frac{V_{condensed}(H_2O)}{V_{stoichiometric}(H_2O)} or \frac{m_{condensed}(H_2O)}{m_{stoichiometric}(H_2O)} \tag{8}$$

Concerning the measurement uncertainty of the conversion the problem of water not fully dropping down into the burette/sample holder needs to be mentioned. For some experiments, the cooler and bridge are weighed after the experiment resulting in losses of water in the system in the range of 0.5–1 ml. Therefore, the measurement uncertainty of the burette (±0.05 ml for 58.9 ml stoichiometric water) and the load cell (±0.27 g for 18.3 g stoichiometric water) are much lower. The maximum conversion is also reliant on the cooling water temperature, which is not constant over the runs, resulting in parts of the water not condensing.

2.4. Heating profile

Slow heating protocols are developed to prevent the lab-scale reactor from overflowing due to excessive foam formation during dehydration. Setup 1a and 1b use the respective heating protocols, shown in Fig. 3 for all experiments to ensure comparability.

Heating protocol Setup 1a. Heating protocol 1a, as seen in Fig. 3(a) is divided into three parts (I – III). In part I the service oil is heated at a 5 K/min heating rate until 150 °C and slows down to 0.5 K/min in part II. When the starting point of heavy foam formation is reached at 175 °C the heating slows further down to 0.2 K/min in part III. Once the heating protocol reaches 215 °C, it maintains this temperature until the dehydration is complete (water stops condensing).

As the reference temperature for the control is the internal temperature of the thermostat, the temperature 1a inside the suspension, presented by the dotted red line in Fig. 3(a) is lower than the theoretical heating curve (blue line). The pinch is around 10 °C, but as soon as the reaction starts, the difference increases to 20 °C since the reaction pulls more heat from the suspension medium than the thermostat can provide. This indicates that the heating power of the thermostat limits the reaction rate. Still, the heating needs to be slowed to prevent the overflowing of the reactor due to foam formation.

Heating protocol Setup 1b. For the extensive cycle stability tests in Setup 1b, the suspension volume is reduced to 240 ml and the heating profile is adjusted to allow faster experiments. In heating protocol 1b, seen in Fig. 3(b), the suspension is heated at a rate of 5 K/min in part I until it reaches 175 °C, after which it is heated at a rate of 0.5 K/min to 215 °C. To ensure more accurate heating rates, the reference temperature has been switched from the internal thermostat temperature to the temperature sensor inside the reactor. As Fig. 3(b) shows, the temperature curve now fits more closely to the desired heating rate, despite the thermostat still having some difficulty in maintaining the temperature during the main reaction phase.

2.5. Equilibrium curves

This work also aims to investigate the influence of pressure on the chemical reactions at hand. Le Chatelier's principle can give a qualitative understanding of how pressure and temperature affect chemical reaction equilibria. It states that a decrease in pressure will favour a reaction that increases volume, while an increase in pressure promotes a reaction that decreases volume [42]. The dehydration of the TCM is accompanied by a significant increase in volume as a gaseous component, water vapour, is formed. This leads to the conclusion that the charging reaction benefits from a decrease in pressure. Since the hydration reaction is performed using liquid water only a slight volume

Table 6
Measuring equipment specifications and their measurement uncertainties.

Parameter	Setup	Location	Equipment	Magnitude of error
Temperature	1a, 2	Reaction zone	Type 'K' Thermocouple (Tolerance class 2)	±2.5 °C
			National Instruments cDAQ-9171	±2°C
Temperature	1b	Reaction zone	PT 100 Thermosensor (Tolerance class AA)	±0.1 °C + 0.0017·T
			B&R temperature module X20 AT B312	±0.0074 %
Conversion	1a	Water collector	Witeg Measuring tube for water estimators, according to Dean Stark, 25 ml, 0.1 ml	±0.05
Conversion	1b	Load cell	Zemic Europe load cell type L6B	±0.02 %
			Zemic Europe Top-Sensors T1 Scale used for calibration	<± 0.1 %
				±0.27 g
System pressure	2	Vacuum pump	Welch Ilmvac Membrane pump VAKUUM SYSTEM LVS 310 Zp economic	±2 mbar
System pressure	2	Reaction zone	Jadpes Universal Fitted Vacuum Pressure Gauge	±4 %

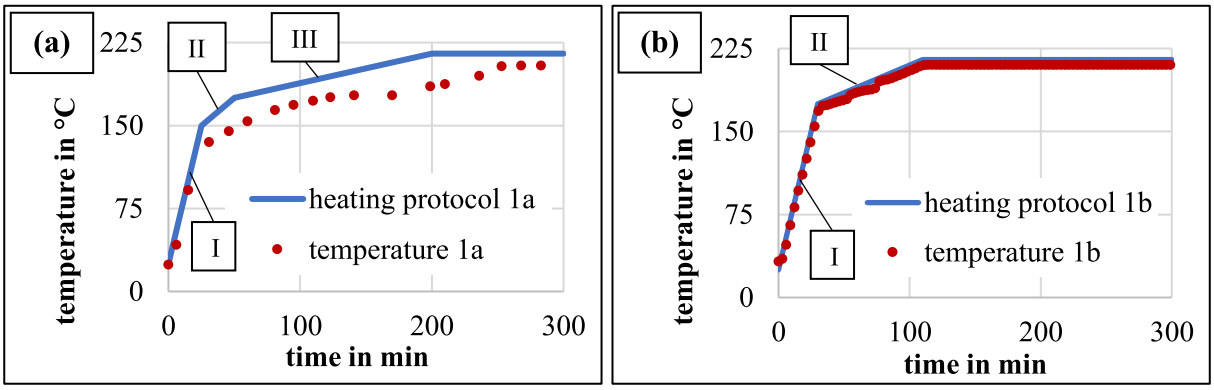

Fig. 3. Heating protocols given to the thermostat and the actual temperature profile inside the reactor in Setup 1a (a) and improved Setup 1b (b).

change occurs, so the influence of pressure is expected to be positive but negligible. Le Chatelier's principle also states that increasing the temperature favours endothermic reactions like the dehydration of the TCM. The equilibrium of the exothermic hydration on the other hand will result from two counteracting forces as lower temperatures favour the exothermic reaction but collision theory still states that higher temperatures will increase the reaction rate [43].

Decreasing the system pressure during charging (dehydration) is expected to lower the reaction starting temperature. The equilibrium's dependence on temperature can be described by the Van't Hoff equation for the equilibrium constant K, which is seen in Eq. (9).

$$lnK = \frac{\Delta_R S^\circ}{R\nu} - \frac{\Delta_R H^\circ}{R\nu T} \tag{9}$$

In the case of the dehydration, the reactants are solid $CaCl_2 \cdot 2\,H_2O$ and gaseous H_2O and the temperature level depends on the water vapour partial pressure p_{H2O}. K can be approximated by $\frac{p_{H2O}}{p^+}$, which results in Eq. (10).

$$ln\left(\frac{p_{H2O}}{p^+}\right) = \frac{\Delta_R S^\circ}{R\nu} - \frac{\Delta_R H^\circ}{R\nu T} \tag{10}$$

In the Equation p^+ refers to the reference pressure (1 bar), while $\Delta_R H^\circ$ and $\Delta_R S^\circ$ are the standard enthalpy and entropy of the reaction, respectively. R represents the universal gas constant, ν the stoichiometric factor for the respective reaction ($\nu = 1$) and T the temperature in K [8]. The equilibrium of the reaction can be plotted as $ln\left(\frac{p_{H2O}}{p^+}\right)$ vs. T^{-1} in 1/K, or for easier understanding as p_{H2O} vs. T in°C. In the suspension reactor, the system pressure is assumed to be approximately equal to the partial pressure of the water p_{H2O} since the suspended particles are surrounded only by water vapour.

2.6. Materials

Calcium chloride dihydrate. The material used in this work is calcium chloride dihydrate of the company Diacleanshop in pharmaceutical purity.

Thermal oils. A suspension medium must meet several criteria to be suitable for the intended application. These are outlined below:

- The medium must be inert towards the TCM.
- The medium must fit the application's temperature range up to 215 °C.
- The medium must exhibit good heat transfer properties.
- The medium must be non-toxic, readily available and inexpensive.

As several thermal oils fit these criteria mineral, silicone, rapeseed and sunflower oil are tested. The tested hydrogenated mineral oil-based heat transfer fluid "FRAGOLTHERM® Q-32-N" (mineral oil) and a polydimethylsiloxane-based heat transfer fluid "FRAGOLTHERM® X-400-A" (silicone oil) were purchased from Fragol AG. The rapeseed/canola oil in question is of the brand "Rapso®", while the sunflower oil "dmBio Bratöl", was obtained from dm-drogerie markt GmbH + Co. KG.

Table 7 gives an overview of important parameters to compare the thermal oils. Especially the price of silicone oil compared to the other oils stands out even when purchased on an industrial scale. The silicone and mineral oil prices were obtained from correspondence with the company Fragol AG and the vegetable oil prices were sourced from stock market web pages.

Mineral oils are produced by distilling crude oil or raw mineral oil materials. Therefore, the chemical structure of FRAGOLTHERM® Q-32-N is mainly composed of paraffinic, naphthenic, and aromatic components. This specific oil is designed as a heat transfer fluid that can withstand temperatures up to 320 °C. Silicone oils like FRAGOLTHERM® X-400-A consist of a periodically alternating arrangement of silicon and oxygen atoms [53]. Despite their polarised chains, they have a low surface tension compared to other oils and exhibit a foam-breaking effect that can also be observed in the suspension reactor. This leads to less foaming in the reactor during the charging reaction when using silicone rather than mineral oil [54].

From a chemical perspective, rapeseed (or canola) oil and sunflower oil are esters of the three-carbon trihydric alcohol glycerine. The main difference between rapeseed and sunflower oil is their fatty acid composition. Both are highly biodegradable and can be considered sustainable, which makes them attractive for use [50]. The main challenge of these oils is their medium oxidation stability and their low hydrolytic stability [52,55].

3. Results and discussion

3.1. Variation of the solid mass fraction

Different solid mass fractions w_{solid} are tested to see the influence on the suspendability, agglomeration, crust formation and conversion during the dehydration. The tested mass fractions are 30, 40, 50, 60 and 70 wt% of $CaCl_2 \cdot 2\,H_2O$ in a mixture of $CaCl_2 \cdot 2\,H_2O$ and mineral oil as Eq. (11) shows.

$$w_{solid} = \frac{m_{CaCl2\bullet 2H2O}}{m_{suspension}} = \frac{m_{CaCl2\bullet 2H2O}}{m_{CaCl2\bullet 2H2O} + m_{mineraloil}} \tag{11}$$

The suspension is heated according to the previously explained heating profile for all mass ratios, as seen in Fig. 3(a). Fig. 4 shows the resulting conversion of the dehydration of $CaCl_2 \cdot 2\,H_2O$ in mineral oil with different solid mass fractions measured in the batch reactor.

The graph only shows a deviation for the experiment using a $w_{solid} =$ 70 wt%. The slower reaction and lower conversion can be explained by the agglomeration and crust formation, causing a decrease in the

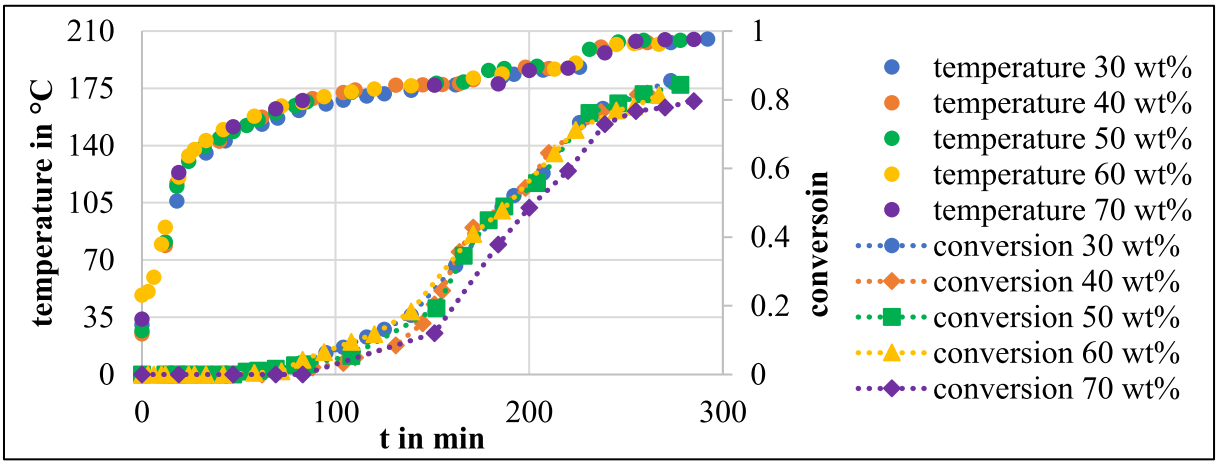

Fig. 4. Conversions of the charging reaction of $CaCl_2 \cdot 2\,H_2O$ in mineral oil at different solid weight fractions.

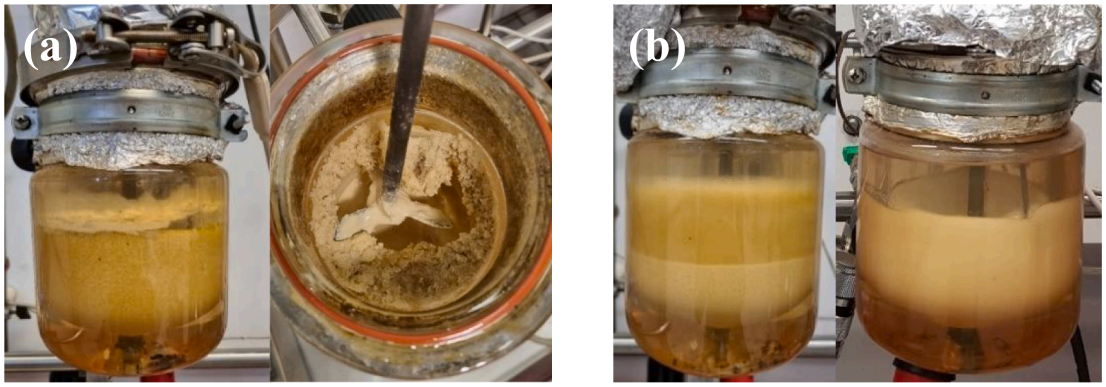

Fig. 5. Crust formation during and after the charging reaction of $CaCl_2 \cdot 2\,H_2O$ with 70 wt% solid mass fraction (a) and 40 wt% solid mass fraction (b) in mineral oil.

Table 7
Overview of the tested thermal oils [44–52].

		Mineral oil	Silicone oil	Rapeseed oil	Sunflower oil
Chemical structure	–	higher alkanes	siloxane	triglycerides	Triglycerides
Price[1]	€/kg	2.37	28	1.14	1.06
Temperature range	°C	< 320	< 200	< 205	< 210
Pourpoint	°C	−12	< −60	−18	−12
Density @25 °C	kg/m^3	868	960	919	919
Viscosity @25 °C	mPas	56.7	48.0	77.6	52.8
Heat capacity@25 °C	kJ/(kgK)	1.99	1.53	1.88	2.07
Thermal conductivity @25 °C	W/(mK)	0.133	0.151	0.169	0.179
Interfacial tension with water @25 °C	mN/m	49.0	34.4	33.5	37.0

[1] Assumed costs at industrial scale.

reactive surface of the TCM. The higher mass fraction makes it harder for the stirrer to fully suspend the particles. Therefore the stirrer speed must be increased to 650 rpm to ensure a homogenous suspension. Nevertheless, the particles agglomerate and form a crust after one dehydration, as Fig. 5(a) shows. Therefore solid mass fractions over 70 wt% are not tested, as this problem will only increase with higher solid weight fractions. When the reaction is done with a $w_{solid} = 40$ wt% (Fig. 5(b)) or lower, neither agglomeration nor crust formation is observed.

Table 8 further explains the results of the tests using different solid mass fractions w_{solid} in the reactor. An influence on the needed stirrer speed to fully suspend the particles and the conversion, agglomeration, and crust formation can be observed.

The higher the solid weight fraction, the higher the stirrer speed needs to be to suspend the particles and the higher the probability for agglomeration and crust formation. This directly causes the maximum conversion to decrease with higher solid content. The uncertainty of the maximum conversion (±0.017 for 58.9 ml stoichiometric water) considers the uncertainty of the burette and that 1 ml of water is lost in the

Table 8
Influence of the solid mass fractions in the reactor on stirrer speed, conversion, agglomeration, and crust formation during the charging of $CaCl_2 \cdot 2\,H_2O$ in mineral oil.

w_{solid}	Stirrer speed	Conversion (±0.017)	Agglomeration	Crust formation
wt%	rpm	–	–	–
70:30	500 – 650	0.796	++	+++
60:40	500 – 650	0.813	++	++
50:50	400 – 450	0.843	++	++
40:60	300 – 450	0.818	none	None
30:70	300 – 450	0.876	none	None

setup as explained in chapter 2.3.

These observations are drawn from two runs with each solid mass fraction. It can be concluded that a solid mass fraction of 30 or 40 wt% is preferred to avoid agglomeration and crust formation while keeping the required stirrer speed low. This information is used in further tests concerning the cycle stability in different suspension media. Lower solid mass fractions than 30 wt% are not tested but are expected to perform equally well. Still, using more oil would increase the needed reactor size and cost in scale-up and should therefore be avoided.

3.2. Comparison of different thermal oils

As described in Chapter 2.2 the cycle stability of the TCM in different thermal oils is tested using the heating protocol 1a and $w_{solid} = 40$ wt%. The stirrer speed is fixed to 400 rpm for all the tests to ensure a homogenous suspension. The amount of condensed water is noted every 5 min to see if there is any change in conversion over five runs. To test several cycles, the amount of condensed water is then added during hydration, plus an additional 1 ml to compensate for losses in the setup. Fig. 6 shows the conversions of the dehydration over five runs in the different oils.

Additionally, the maximum temperature rise during the hydration is noted. Table 9 and Fig. 7 show the maximum dehydration conversion (again with ±0.017 uncertainty) and the maximum hydration temperature rise over the five runs in the different oils. The temperature measurement using the type K element has an accuracy of ±4.5 °C but the values should still be comparable as all measurements were taken using the same measurement equipment.

Mineral oil. Fig. 6 shows that conversion curves overlap, suggesting a stable reaction throughout the cycles in mineral oil. The maximum temperature needed to reach over 0.8 conversion within 400 min in mineral oil is 205 °C in the suspension which requires 210 °C in the service oil pump. The start of the reaction is accompanied by heavy foaming each run. The maximum conversion and temperature rise shown in Fig. 7, also show no worsening trend over the runs.

Silicone oil. In silicone oil, a slight worsening trend in the conversion can be observed in both Fig. 6 and Fig. 7(a). In the first three runs, the conversion is higher than in mineral oil, which is likely caused by a better heat transfer since the suspension temperature is higher, even though the temperature profile in the thermostat is the same. This is likely caused by the higher thermal conductivity of 0.151 W/(mK) compared to 0.133 W/(mK) for mineral oil. Due to the silicone oil's lower interfacial tension with water (s. Table 7) less foaming is observed. In the fourth and fifth runs, the conversion drops below 0.85 caused by slight agglomeration starting in the third run and crust formation on the reactor wall observed from the fourth run onwards. Fig. 7 (b) shows a higher temperature rise in silicone oil than the other oils, caused by the lower specific heat capacity of the oil (s. Table 7). However, it also shows a slight decreasing trend for the temperature rise over the runs. This is also caused by the decrease in the reactive surface due to agglomeration and crust build-up. In general, the particles agglomerate more during discharging in silicone oil than in mineral oil. The stirrer speed must be partially increased to 500 rpm to ensure a homogenous suspension despite agglomeration. The agglomeration of the particles in silicone oil could be caused by the operation temperature of 210 °C being over the recommended temperature range of the oil (<200 °C).

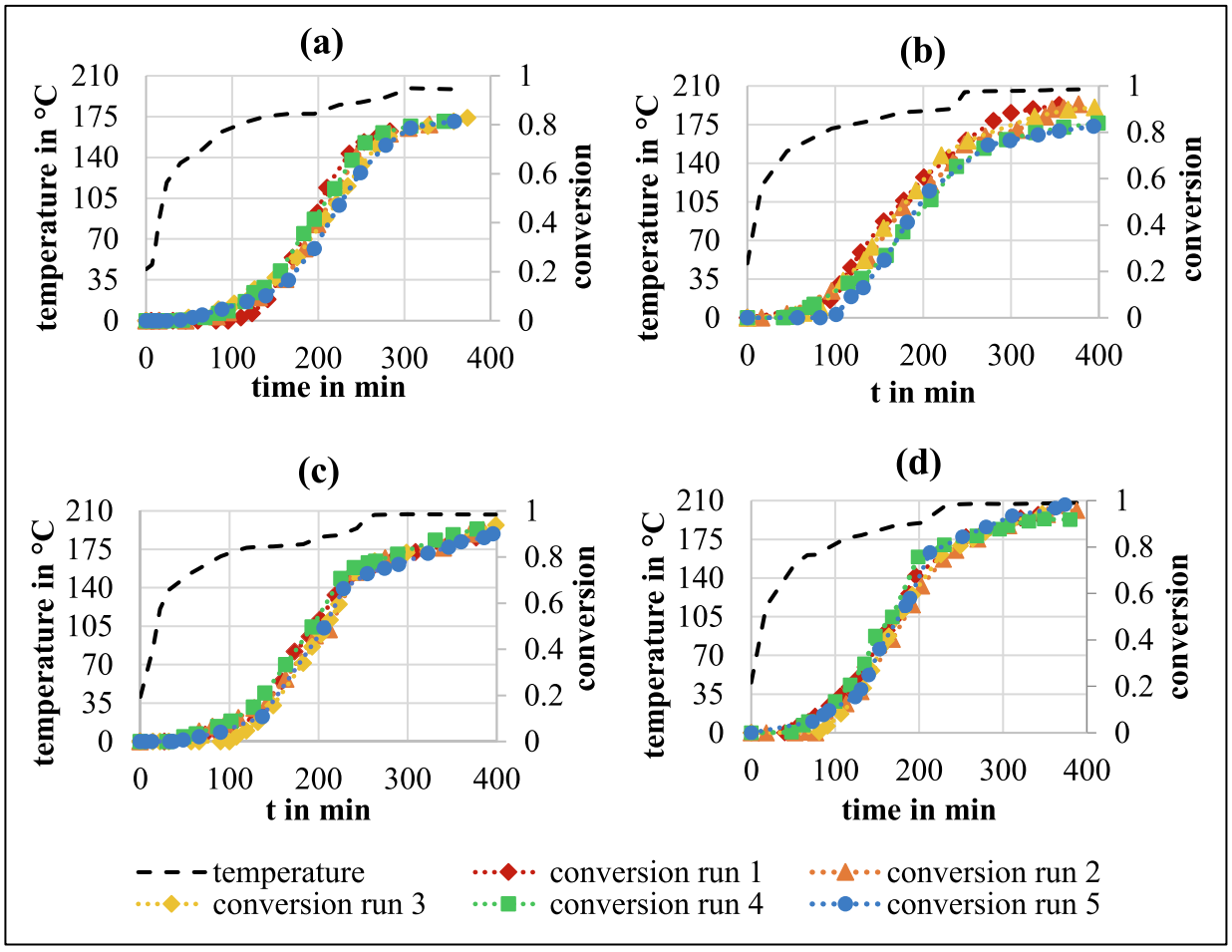

Fig. 6. Conversion curves and temperature in the suspension for five dehydration runs in mineral oil (a), silicone oil (b), rapeseed oil (c) and sunflower oil (d) (40 wt % solid).

Table 9
Maximum conversion during dehydration and maximum temperature rise during hydration over five runs in different thermal oils (40 wt% solid).

Thermal oil	$conversion_{dehydration}$ (±0.017)					$\Delta T_{hydration}$ in°C (±4.5 °C)				
	Run 1	Run 2	Run 3	Run 4	Run 5	Run 1	Run 2	Run 3	Run 4	Run 5
Mineral	0.818	0.801	0.829	0.815	0.815	13.3	19.2	17.2	16.1	17.7
Silicone	0.918	0.921	0.907	0.840	0.826	28.3	23.7	24.6	22.1	22.7
Rapeseed	0.884	0.918	0.938	0.921	0.901	19.2	19.4	19.4	21.2	18.7
Sunflower	0.939	0.958	0.944	0.918	0.982	19.3	18.6	24.1	26.2	27.5

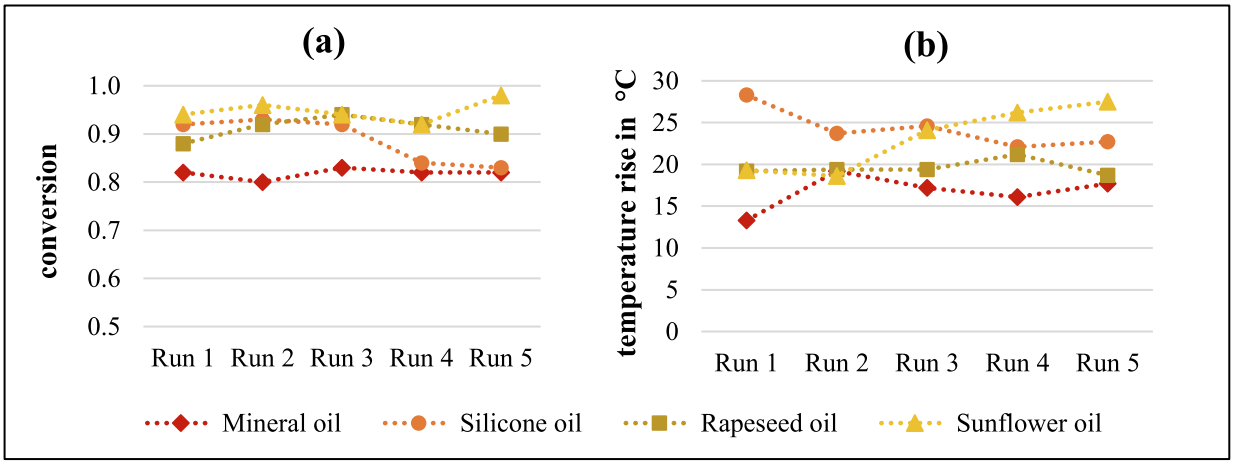

Fig. 7. Maximum conversion during dehydration (a) and maximum temperature rise during hydration (b) over five runs in different thermal oils (40 wt% solid).

Rapeseed oil. As Fig. 6 and Fig. 7(a) show, the conversion stays the same over five runs reaching over 0.9 in all runs but the first. Compared to the curves produced using mineral and silicone oil, the conversion curves in rapeseed oil have a change of slope that shows the start of the second reaction step. As for silicone oil, the superior heat transfer due to a higher thermal conductivity (s. Table 7) and the resulting higher temperature in the suspension can explain the higher conversion than in mineral oil. No agglomeration or crust formation is observed, and foaming is initially less than in mineral oil which corresponds to the lower interfacial tension with water. In the fourth run foaming increases, suggesting that the surface tension of the oil changes. This is most likely caused by degradation of vegetable oil being heated in the presence of oxygen and water. The oil also changes colour and smell, suggesting that it becomes rancid. At 210 °C the application requires higher temperatures than the recommended temperature range of the rapeseed oil (<205 °C) which explains the rapid aging. Still, the results in Fig. 7 show stable dehydration and hydration reactions over five runs.

Sunflower oil. Similar to rapeseed oil, the two reaction steps in sunflower oil can be distinguished by a change of slope in the conversion curve in Fig. 6. The reached maximum conversion is the highest of all oils at over 0.9 each run, even reaching 0.982±0.017 in run five, as seen in Table 9 and Fig. 7(a). The results of the dehydration experiments suggest stable cycles. During hydration, however, the temperature rise (Fig. 7(b)) increases from run three onwards. That suggests a change in the oil parameters like the specific heat capacity, possibly rooted in degradation due to the high temperature. No agglomeration or crust formation occurs, but the foaming, which is not apparent in run one, increases in runs two to four and then stops again in run five. The inconsistent foaming undermines the assumption that the oil is changing and becoming rancid. Like rapeseed oil, it changes colour and begins to smell.

Comparison. The tests show that calcium chloride dihydrate can be used as a TCM in the suspension reactor in all the tested oils. It does not appear to react with any of the oils and cycle stability is given to an extent, but differences in performance can be seen. The effects on different parameters are summarised in Table 10. The oil seems to impact the conversion, probably due to differences in thermal conductivity and the thereby caused suspension temperature. It also impacts the temperature rise in the suspension due to the differences in specific heat capacity. Silicone oil is the only oil showing a worsening trend in both charging and discharging over five runs. This is caused by agglomeration and crust formation, which even needs an increase in stirrer speed, as Table 10 shows.

On the upside, silicone oil has lower surface tension and inhibits foaming. Fig. 8 shows the foam formation during charging in mineral oil (a) and silicone oil (b). There is noticeably less foaming in silicone oil. The white line and arrows indicate the height of the foam layer in the reactor. The pictures are taken during charging but with a turned-off

Table 10
Summarised effects of the tested oils on different parameters.

Thermal oil	Stirrer speed	Foaming[1]	Agglo-meration	Crust formation	Max. conversion (±0.017)	max. ΔT_{hydr} (±4.5°C)
	Rpm					°C
Mineral oil	400	++	–	–	0.829	19.2
Silicone oil	400–500	+	+	+	0.921	28.3
Rapeseed oil	400	+/++[2]	–	–	0.938	21.2
Sunflower oil	400	–/++[3]	–	–	0.982	27.5

[1] ++: ~5 cm foam layer, +: ~1 cm foam layer, –: no foam.
[2] + run 1–3 and ++ run 4–5.
[3] – run 1 and 5 and ++ run 2–4.

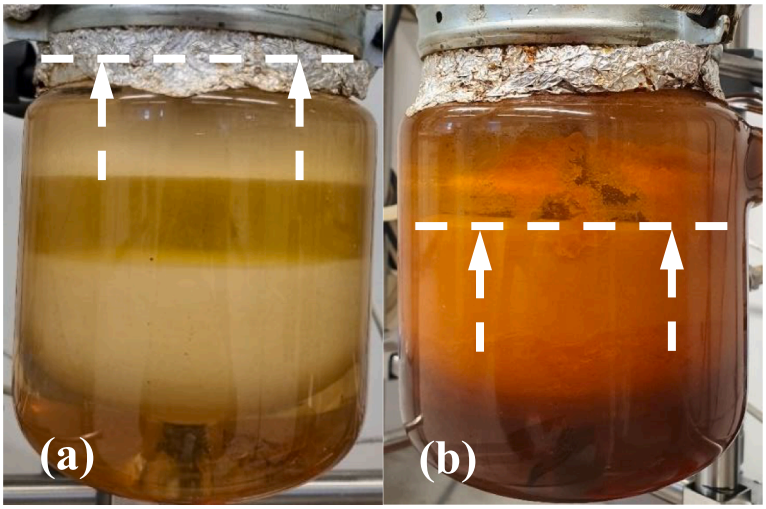

Fig. 8. Foaming of $CaCl_2 \cdot 2\,H_2O$ during the dehydration in mineral oil (a) and silicone oil (b) – not stirred.

stirrer.

Calcium chloride dihydrate shows potential to be used as a TCM in a suspension reactor using vegetable oils. The highest conversion during the charging reaction and the highest (maximum) temperature rise during discharging can be reached using sunflower oil. However, due to their low oxidation and hydrolytic stability, their cycle stability could be negatively affected over multiple runs. Rapeseed oil still shows very consistent results over the five runs for both dehydration and hydration.

Due to its high temperature range (<320 °C) mineral oil shows good cycle stability and no signs of degradation over five cycles. Additionally, it does not cause agglomeration or crust formation, only the foaming requires a solution.

3.3. Extensive tests in mineral oil

Mineral oil is tested extensively in Setup 1b (s. Chapter 2.2) over 25 dehydration-hydration cycles to further check its stability, as it showed the most potential regarding cycle stability in previous tests. A mass fraction of 30 wt% is chosen to further minimise agglomeration, crust formation and foaming. The faster heating profile 1b (s. Fig. 3) increases the reaction rate and the reaction finishes after 270 min instead of 400 min. The first part of the reaction starting at 170 °C takes around 60 min until a change in the slope occurs once the suspension reaches 195 °C. This indicates that the faster first reaction step has slowed down and the slower second reaction step takes over. This is caused by the fact that the suspension temperature is much closer to the equilibrium temperature of the second step.

As Fig. 9 and Fig. 10(a) show, the conversion of the dehydration reaction is stable for the 25 investigated runs. The calculation of the curves at +/− two times the standard deviation over all 25 runs and the plot of every 5th run in Fig. 9 suggest that there is no clear trend towards a lower reaction rate or a decrease in maximum conversion over the runs. Fig. 11 and Fig. 10(b) show the temperature rise during dehydration which appears stable over 22 runs, only increasing slightly which can be explained by the 0.5–1 ml of oil which is lost and collected in the cooler each run. As the measurement starts at room temperature (23.7 to 24.7 °C ± 4.5 °C) the maximum temperature results in 35.2 to 40.6 °C (±4.5 °C). In the last three runs the temperature increases significantly which could be explained by some oil leaking from the bottom of the reactor but could also be a sign that the material properties of the oil are beginning to change. The uncertainty of the maximum conversion shown in Fig. 10(a) again considers the accuracy of the load cell and assumes 1 ml water is lost in the system, resulting in ±0.07.

Fig. 11 also shows the boundaries of 95 % of the curves between run 1 and 22, with run 23–25 being excluded as outliers. Again every 5th run is plotted to show the progression over the runs which again does not show a clear trend except for run 23–25.

In the improved Setup 1b the temperature measurement provides an accuracy of around +/−0.3 °C in the considered temperature range but the losses of the non-insulated reactor are visible in the graphs.

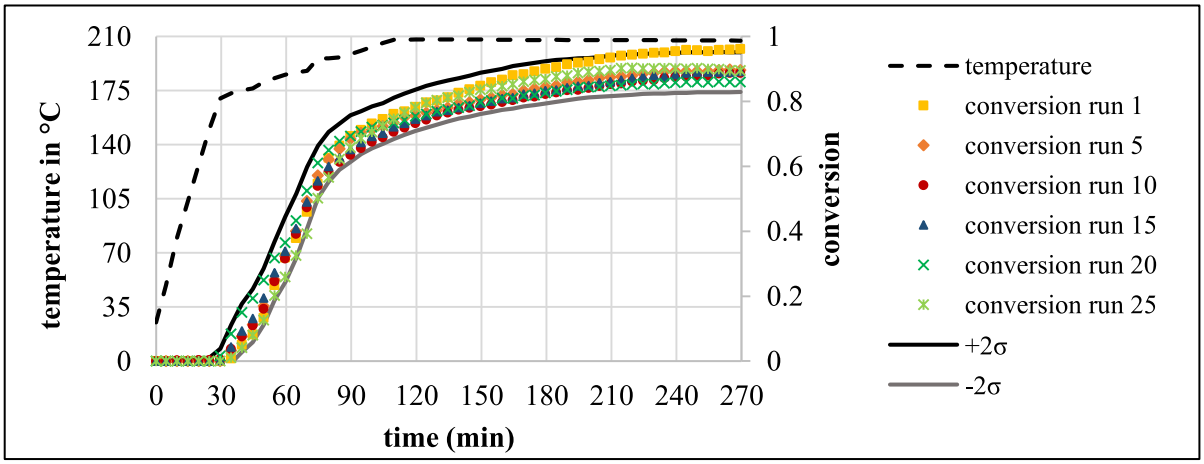

Fig. 9. Conversion curves and temperature profile for 25 runs of the dehydration of $CaCl_2 \cdot 2\,H_2O$ in mineral oil (30 wt% solid).

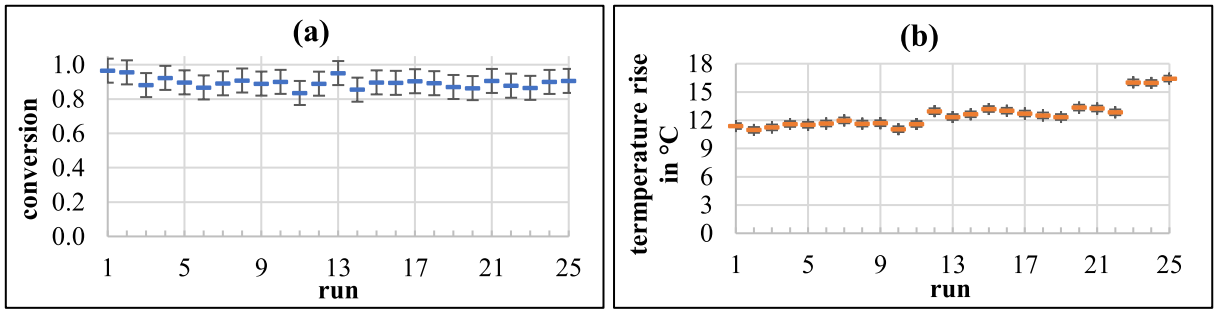

Fig. 10. Conversion of the dehydration (a) and temperature rise during the hydration (b) of $CaCl_2 \cdot 2\,H_2O$ in mineral oil (30 wt% solid) over 25 runs.

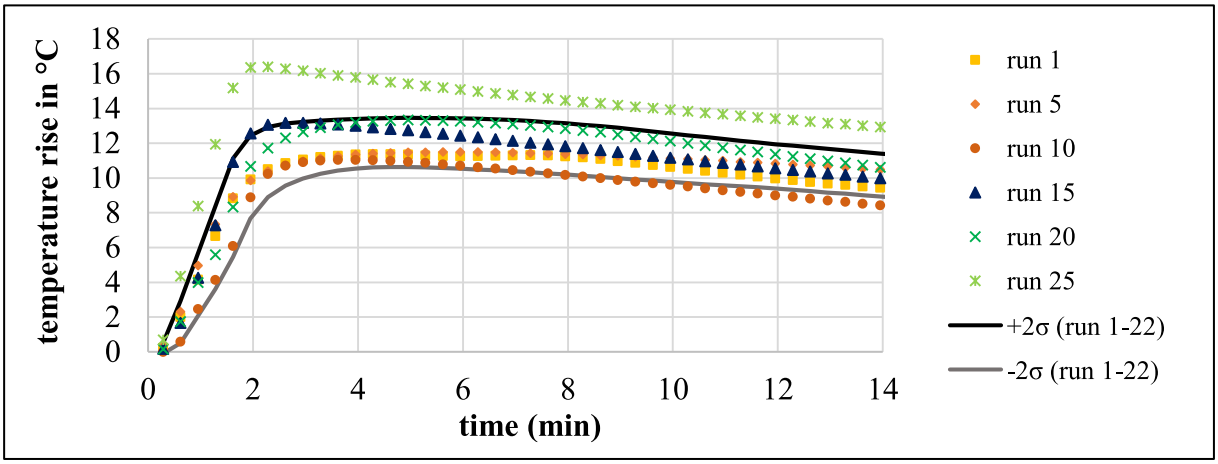

Fig. 11. Temperature rise for 25 runs of the hydration of $CaCl_2$ in mineral oil (30 wt% solid).

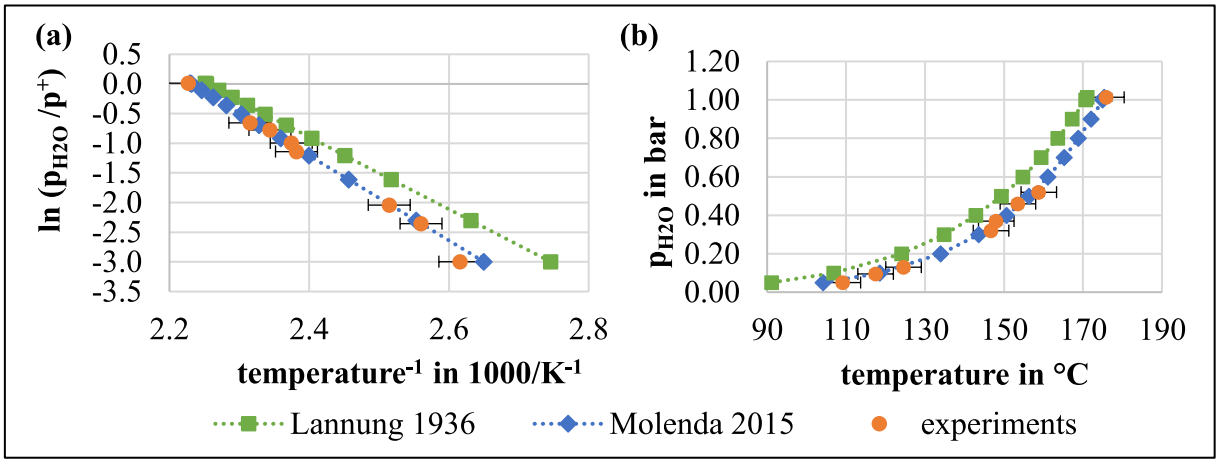

Fig. 12. Classical Van't Hoff plots (a) and pT-curves (b) of the reaction of $CaCl_2 \cdot 2\,H_2O$ to $CaCl_2{\cdot}H_2O$ [16,56].

However, a worsening trend over the first 20 runs is not apparent, except for the outlier run 25. The plots also show that the hydration reaction is up to 50 times faster than the dehydration in the suspension, taking <5 min to reach the maximum temperature.

3.4. Influence of pressure

Fig. 12 shows the influence of system pressure on the starting temperature of the dehydration of $CaCl_2 \cdot 2\,H_2O$. The values are obtained by heating the suspension in the three-necked flask setup while setting the system pressure using an internally controlled vacuum pump. The starting temperature is determined as the temperature at which the first bubbles are formed in the suspension, which is visually judged.

The obtained data can be compared to literature by using values for $\Delta_R S^\circ$ and $\Delta_R H^\circ$ obtained from other papers or thermodynamic databases and putting them into Eqs. (3) and (4). This way, the pT-curves seen in Fig. 12 are created, allowing the experimental data to be compared to them.

Of the chosen thermodynamic data sets that are used to calculate the curves, one was obtained by doing experiments in a fixed bed reactor by *Molenda et al.* [16], while the other one was derived from vapour pressure measurements with a hot-wire manometer done by *Lannung* [56]. The experimental data obtained in the suspension corresponds very closely to the data from *Molenda et al.* [16]. The two data sets present the

Table 11
Comparison of the starting temperature of the dehydration of $CaCl_2 \cdot 2\,H_2O$ at lower system pressures.

$CaCl_2 \cdot 2\,H_2O \leftrightarrow CaCl_2 + 2\,H_2O$	
p (±2 mbar)	T_{start} (±4.5 °C)
mbar	°C
1013	175.92
520	158.80
460	153.51
370	148.03
320	146.70
130	124.54
95	117.47
50	109.17

differences in thermodynamic measurements depending on how they were obtained.

Table 11 compares the starting temperatures of the charging reaction at ambient pressure and different lower pressures. It is apparent that by lowering the pressure, the starting temperature of the dehydration reaction can be lowered significantly, allowing the system to be charged with a lower temperature heat.

3.5. Constraints of the setup and considerations for future experiments

The current experimental setup does not permit the determination of the true reaction kinetics, as the water vapour must first leave the suspension, move further towards the cooler, and then drip down into the burette or sample holder to be recognised by the measurement system. Nevertheless, the experiments can indicate the magnitude of the reaction rate. The experiments reveal that the dehydration experiments take several hours and are therefore very slow compared to the hydration reaction which stops after a few minutes. Previous theoretical investigations on a similar salt hydrate reaction (the dehydration of calcium oxalate monohydrate) in a suspension suggest that the mass transfer of water vapour in oil can heavily limit the reaction rate. If the water vapour bubbles are too small the mass transfer no longer proceeds via bubble rising but solely by diffusion which increases the reaction time from the range of seconds to hours [57]. To increase the bubble size the nitrogen stream could be added at the bottom of the reactor instead of the top to promote coalescence. Additionally, the formation of foam further hinders the water from exiting the suspension so foam mitigation should be a focus. Solving the foaming problem would also allow a faster heating rate which would increase the reaction rate in the batch reactor. On a larger scale, the reactor should be operated continuously and at a constant temperature which will further increase the reaction rate since the preheating phase is skipped.

4. Conclusion

Creating a suitable heating profile to perform comparable cycles in the batch-type reactor makes it possible to test the stability of several dehydration-hydration cycles of calcium chloride dihydrate in a three-phase suspension reactor. Different mass fractions of the solid reactant $CaCl_2 \cdot 2\,H_2O$ in the inert liquid (thermal oil) are investigated, rendering a solid mass fraction of 40 wt% or lower as the most promising to avoid agglomeration and maximise the conversion of the dehydration reaction. At ambient pressure, the reversibility of the reaction is tested for five cycles in different suspension media. Out of the tested thermal oils, the vegetable oils show the best results regarding agglomeration, crust formation and heat release during hydration. Additionally, they result in the highest conversion at a maximum of 0.938–0.982±0.017 compared to the 0.829±0.017 and 0.921±0.017 obtained in mineral oil and silicone oil respectively. This is attributed to improved heat transfer due to higher thermal conductivity resulting in higher suspension temperatures. The application of these oils is questionable due to thermal degradation in the presence of oxygen and water, which can be observed over five cycles. The results still suggest five stable cycles in rapeseed oil which requires further investigation. Mineral oil is the most promising oil regarding thermostability, given its high-temperature range. It also exhibits cycle stability, which is further proven in 22 stable dehydration-hydration cycles. The investigation of the dehydration behaviour at lower system pressures (down to 50 mbar) shows a significant shift of the reaction temperatures to lower values (e.g. the starting temperature decreases from 175±4.5 °C at ambient pressure to 109±4.5 °C at 50±2 mbar). This could create new waste heat potentials that can be stored using calcium chloride dihydrate.

It can be concluded that calcium chloride shows a high potential for use in this type of reactor concept, especially in mineral oil. For future experiments, a focus on improving the mass transfer of the vapour out of the suspension is imperative as well as finding a solution for excessive foaming.

Declaration of competing interest

The authors declare that they have no known competing financial interests or personal relationships that could have appeared to influence the work reported in this paper.

Data availability

Data will be made available on request.

Acknowledgements

Funding: This project has received funding from the European Union's Horizon 2020 research and innovation program under grant agreement No 101036766. The authors acknowledge TU Wien Bibliothek for financial support through its Open Access Funding Programme.

References

[1] IEA, "Renewables 2020," Paris, 2020. Accessed: Apr. 22, 2024. [Online]. Available: https://www.iea.org/reports/renewables-2020.
[2] G. Bianchi, et al., Estimating the waste heat recovery in the European Union Industry, Energy Ecol Environ 4 (5) (2019) 211–221, https://doi.org/10.1007/s40974-019-00132-7.
[3] C. Forman, I.K. Muritala, R. Pardemann, B. Meyer, Estimating the global waste heat potential, Renew. Sustain. Energy Rev. 57 (2016) 1568–1579, https://doi.org/10.1016/j.rser.2015.12.192.
[4] I. Hayatina, A. Auckaili, M. Farid, Review on the Life Cycle Assessment of Thermal Energy Storage Used in Building Applications, Energies (basel) 16 (3) (2023) 1170, https://doi.org/10.3390/en16031170.
[5] P. Kalita, D. Kashyap, U. Bordoloi, "Thermal Energy Storage Systems for Cooling and Heating Applications", in *Energy Storage*, Wiley (2021) 149–199, https://doi.org/10.1002/9781119555599.ch5.
[6] F. Desai, J. Sunku Prasad, P. Muthukumar, and M. M. Rahman, "Thermochemical energy storage system for cooling and process heating applications: A review," *Energy Conversion and Management*, vol. 229. Elsevier Ltd, Feb. 01, 2021. doi: 10.1016/j.enconman.2020.113617.
[7] R. Salgado-Pizarro, A. Calderón, A. Svobodova-Sedlackova, A.I. Fernández, C. Barreneche, The relevance of thermochemical energy storage in the last two decades: The analysis of research evolution, J Energy Storage 51 (2022), https://doi.org/10.1016/j.est.2022.104377.
[8] M. Richter, E.-M. Habermann, E. Siebecke, M. Linder, A systematic screening of salt hydrates as materials for a thermochemical heat transformer, Thermochim Acta 659 (2018) 136–150, https://doi.org/10.1016/j.tca.2017.06.011.
[9] O. Kizilkan, I. Dincer, Borehole thermal energy storage system for heating applications: Thermodynamic performance assessment, Energy Convers Manag 90 (2015) 53–61, https://doi.org/10.1016/j.enconman.2014.10.043.
[10] P. Fleuchaus, B. Godschalk, I. Stober, P. Blum, Worldwide application of aquifer thermal energy storage – A review, Renew. Sustain. Energy Rev. 94 (2018) 861–876, https://doi.org/10.1016/j.rser.2018.06.057.
[11] L.F. Cabeza, "Advances in thermal energy storage systems: Methods and applications", in *Advances in Thermal Energy Storage Systems Methods and Applications*, Elsevier (2020) 37–54, https://doi.org/10.1016/B978-0-12-819885-8.00002-4.
[12] E. Palomo Del Barrio, R. Cadoret, J. Daranlot, F. Achchaq, New sugar alcohols mixtures for long-term thermal energy storage applications at temperatures

between 70°C and 100°C, Sol. Energy Mater. Sol. Cells 155 (2016) 454–468, https://doi.org/10.1016/j.solmat.2016.06.048.
[13] A. Solé, I. Martorell, L.F. Cabeza, State of the art on gas–solid thermochemical energy storage systems and reactors for building applications, Renew. Sustain. Energy Rev. 47 (2015) 386–398, https://doi.org/10.1016/j.rser.2015.03.077.
[14] ECHA, "European Chemicals Agency." Accessed: Sep. 22, 2023. [Online]. Available: https://echa.europa.eu/de/informationon-chemicals.
[15] P.A.J. Donkers, L.C. Sögütoglu, H.P. Huinink, H.R. Fischer, O.C.G. Adan, A review of salt hydrates for seasonal heat storage in domestic applications, Appl Energy 199 (2017) 45–68, https://doi.org/10.1016/j.apenergy.2017.04.080.
[16] M. Molenda, J. Stengler, M. Linder, A. Wörner, Reversible hydration behavior of CaCl2 at high H2O partial pressures for thermochemical energy storage, Thermochim Acta 560 (2013) 76–81, https://doi.org/10.1016/j.tca.2013.03.020.
[17] R. Kemp and S. E. Keegan. Calcium Chloride. In *Ullmann's Encyclopedia of Industrial Chemistry*, Weinheim, Germany: Wiley-VCH Verlag GmbH & Co. KGaA, 2000. doi: 10.1002/14356007.a04_547.
[18] Outotec, "HSC Chemistry." 2007.
[19] R. J. Clark, A. Mehrabadi, and M. Farid, "State of the art on salt hydrate thermochemical energy storage systems for use in building applications," *Journal of Energy Storage*, vol. 27. Elsevier Ltd, Feb. 01, 2020. doi: 10.1016/j.est.2019.101145.
[20] A. Barsk, M.R. Yazdani, A. Kankkunen, A. Seppälä, Exceptionally high energy storage density for seasonal thermochemical energy storage by encapsulation of calcium chloride into hydrophobic nanosilica capsules, Sol. Energy Mater. Sol. Cells 251 (2023), https://doi.org/10.1016/j.solmat.2022.112154.
[21] W. Li, J.J. Klemeš, Q. Wang, M. Zeng, Salt hydrate–based gas-solid thermochemical energy storage: Current progress, challenges, and perspectives, Renew. Sustain. Energy Rev. 154 (2022) 111846, https://doi.org/10.1016/j.rser.2021.111846.
[22] V. Palomba, A. Frazzica, Recent advancements in sorption technology for solar thermal energy storage applications, Sol. Energy 192 (2019) 69–105, https://doi.org/10.1016/j.solener.2018.06.102.
[23] E. Courbon, et al., Further improvement of the synthesis of silica gel and CaCl2 composites: Enhancement of energy storage density and stability over cycles for solar heat storage coupled with space heating applications, Sol. Energy 157 (2017) 532–541, https://doi.org/10.1016/j.solener.2017.08.034.
[24] T. Nonnen, et al., A Thermochemical Long-Term Heat Storage System Based on a Salt/Zeolite Composite, Chem Eng Technol 39 (12) (2016) 2427–2434, https://doi.org/10.1002/ceat.201600301.
[25] D. Aydin, S.P. Casey, X. Chen, S. Riffat, Novel 'open-sorption pipe' reactor for solar thermal energy storage, Energy Convers Manag 121 (2016) 321–334, https://doi.org/10.1016/j.enconman.2016.05.045.
[26] S.P. Casey, D. Aydin, J. Elvins, S. Riffat, Salt impregnated desiccant matrices for 'open' thermochemical energy conversion and storage – Improving energy density utilisation through hygrodynamic & thermodynamic reactor design, Energy Convers Manag 142 (2017) 426–440, https://doi.org/10.1016/j.enconman.2017.03.066.
[27] D. Aydin, S.P. Casey, X. Chen, S. Riffat, Numerical and experimental analysis of a novel heat pump driven sorption storage heater, Appl Energy 211 (2018) 954–974, https://doi.org/10.1016/j.apenergy.2017.11.102.
[28] H.U. Rammelberg, T. Osterland, B. Priehs, O. Opel, W.K.L. Ruck, Thermochemical heat storage materials – Performance of mixed salt hydrates, Sol. Energy 136 (2016) 571–589, https://doi.org/10.1016/j.solener.2016.07.016.
[29] M. Gaeini, A.L. Rouws, J.W.O. Salari, H.A. Zondag, C.C.M. Rindt, Characterization of microencapsulated and impregnated porous host materials based on calcium chloride for thermochemical energy storage, Appl Energy 212 (2018) 1165–1177, https://doi.org/10.1016/j.apenergy.2017.12.131.
[30] B.G.P. van Ravensteijn, et al., Encapsulation of Salt Hydrates by Polymer Coatings for Low-Temperature Heat Storage Applications, ACS Appl Polym Mater 3 (4) (2021) 1712–1726, https://doi.org/10.1021/acsapm.0c01186.
[31] A. Palacios, C. Barreneche, M.E. Navarro, Y. Ding, Thermal energy storage technologies for concentrated solar power – A review from a materials perspective, Renew Energy 156 (2020) 1244–1265, https://doi.org/10.1016/j.renene.2019.10.127.
[32] G. Sadeghi, "Energy storage on demand: Thermal energy storage development, materials, design, and integration challenges," *Energy Storage Materials*, vol. 46. Elsevier B.V., pp. 192–222, Apr. 01, 2022. doi: 10.1016/j.ensm.2022.01.017.
[33] W. Hua, H. Yan, X. Zhang, X. Xu, L. Zhang, and Y. Shi, "Review of salt hydrates-based thermochemical adsorption thermal storage technologies," *Journal of Energy Storage*, vol. 56. Elsevier Ltd, Dec. 15, 2022. doi: 10.1016/j.est.2022.106158.
[34] W. Reschetilowski, Ed., *Handbuch Chemische Reaktoren*. Berlin, Heidelberg: Springer Berlin Heidelberg, 2020. doi: 10.1007/978-3-662-56434-9.
[35] H. Zondag *et al.*, "Comparison of reactor concepts for thermochemical storage of solar heat," 2008.
[36] Y. Zhang, R. Wang, Sorption thermal energy storage: Concept, process, applications and perspectives, Energy Storage Mater 27 (2020) 352–369, https://doi.org/10.1016/j.ensm.2020.02.024.
[37] T. Yan, R.Z. Wang, T.X. Li, L.W. Wang, I.T. Fred, A review of promising candidate reactions for chemical heat storage, Renew. Sustain. Energy Rev. 43 (2015) 13–31, https://doi.org/10.1016/j.rser.2014.11.015.
[38] M. Bouché, M. Richter, M. Linder, Heat transformation based on CaCl2/H2O - Part B: Open operation principle, Appl Therm Eng 102 (2016) 641–647, https://doi.org/10.1016/j.applthermaleng.2016.03.102.
[39] M. Richter, M. Bouché, M. Linder, Heat transformation based on CaCl2/H2O - Part A: Closed operation principle, Appl Therm Eng 102 (2016) 615–621, https://doi.org/10.1016/j.applthermaleng.2016.03.076.
[40] National Center for Biotechnology Information, "PubChem Compound Summary for CID 5284359, Calcium Chloride." Accessed: May 16, 2024. [Online]. Available: https://pubchem.ncbi.nlm.nih.gov/compound/Calcium-Chloride#section=Density.
[41] G. Wedl, L. Schmieder, C. Hein, F. Winter, Continuously stirred tank reactor for oil-suspended thermochemical energy storage systems for CuSO4·5H2O, Appl Therm Eng 255 (Oct. 2024) 123977, https://doi.org/10.1016/j.applthermaleng.2024.123977.
[42] H. Bannwarth, B. P. Kremer, and A. Schulz, *Basiswissen Physik, Chemie und Biochemie*. Berlin, Heidelberg: Springer Berlin Heidelberg, 2019. doi: 10.1007/978-3-662-58250-3.
[43] K.J. Laidler, A glossary of terms used in chemical kinetics, including reaction dynamics (IUPAC Recommendations 1996), Pure Appl. Chem. 68 (1996) 149–192.
[44] Y. Cong, W. Zhang, C. Liu, and F. Huang. Composition and Oil-Water Interfacial Tension Studies in Different Vegetable Oils. DOI: 10.1007/s11483-019-09617-8/ Published.
[45] F. Peters, D. Arabali, Interfacial tension between oil and water measured with a modified contour method, Colloids Surf A Physicochem Eng Asp 426 (2013) 1–5, https://doi.org/10.1016/j.colsurfa.2013.03.010.
[46] H. Kim, D.J. Burgess, Prediction of interfacial tension between oil mixtures and water, J Colloid Interface Sci 241 (2) (2001) 509–513, https://doi.org/10.1006/jcis.2001.7655.
[47] Fragol AG. Produktinformation FRAGOLTHERM ® X-400-A (vormals FRAGOLTHERM ® X-BF). 2021.
[48] Fragol AG. Produktinformation FRAGOLTHERM ® Q-32-N. 2021.
[49] Trading Economics, "Sunflower oil price," 2023, Accessed: Mar. 05, 2023. [Online]. Available: https://tradingeconomics.com/commodity/sunflower-oil.
[50] E.E.G. Rojas, J.S.R. Coimbra, J. Telis-Romero, Thermophysical properties of cotton, canola, sunflower and soybean oils as a function of temperature, Int J Food Prop 16 (7) (2013) 1620–1629, https://doi.org/10.1080/10942912.2011.604889.
[51] Neste, "Palm and rapeseed oil prices." Accessed: Mar. 05, 2023. [Online]. Available: https://www.neste.com/investors/market-data/palm-and-rapeseed-oil-prices.
[52] N. A. Bin Masripan *et al.*, "Vegetable Oil as Bio-Lubricant and Natural Additive in Lubrication: A Review," 2020. [Online]. Available: https://api.semanticscholar.org/CorpusID:222476805.
[53] R. Schliebs and J. Ackermann, *Chemie und Technologie der Silicone I*, vol. 21. 1987. doi: 10.1002/ciuz.19870210404.
[54] D.-C. Christian, F. Aus, K. Bayreuth, Untersuchungen Zur Stabilität Von Tensidschäumen (2006).
[55] A.W. Girotti, Mechanisms of Lipid Peroxidation, J Free Radic Biol Med I (1985) 87–95.
[56] A. Lannung, Dampfdruckmessungen des Systems Calciumchlorid-Wasser, Zeitschrift Fr Anorganische Und Allgemeine Chemie 228 (1) (1936) 1–18, https://doi.org/10.1002/zaac.19362280102.
[57] L. Garofalo, F.V. Vitiello, F. Montagnaro, H. Bürgmayr, F. Winter, Salt Hydrates for Thermochemical Storage of Solar Energy: Modeling the Case Study of Calcium Oxalate Monohydrate Dehydration/Rehydration under Suspension Reactor Conditions, Ind Eng Chem Res 60 (30) (2021) 11357–11372, https://doi.org/10.1021/acs.iecr.1c01220.